THE JOURNAL OF PHYSICAL CHEMISTRY Letters

Letter

pubs.acs.org/JPCL

Solvent Degradation in Nonaqueous Li-O_2 Batteries: Oxidative Stability versus H-Abstraction

Abhishek Khetan,[†] Heinz Pitsch,[†] and Venkatasubramanian Viswanathan*[,‡]

[†]Institute for Combustion Technology, RWTH Aachen University, Aachen 52056, Germany

[‡]Department of Mechanical Engineering, Carnegie Mellon University, Pittsburgh, Pennsylvania 15213, United States

Supporting Information

ABSTRACT: Developing rechargeable Li-O_2 batteries hinges on identifying stable solvents resistant to decomposition. Here, we focus on solvent stability against adsorption-induced H-abstraction during discharge. Using a detailed thermodynamic analysis, we show that a solvent's propensity to resist H-abstraction is determined by its acid dissociation constant, pK_a, in its own environment. Upon surveying hundreds of solvents for their pK_a values in different media, we find linear correlations between the pK_a values across various classes of solvents in any two given media. Utilizing these correlations, we choose DMSO as the common standard to compare the relative stability trends. We construct a stability plot based on the solvent's HOMO level and its pK_a in DMSO, which reveals that most solvents obey a correlation where solvents with lower HOMO levels tend to have lower pK_a values in DMSO. However, this is at odds with the stability requirement that demands deep HOMO levels and high pK_a values. Thus, stable solvents need to be outliers to this observed correlation.

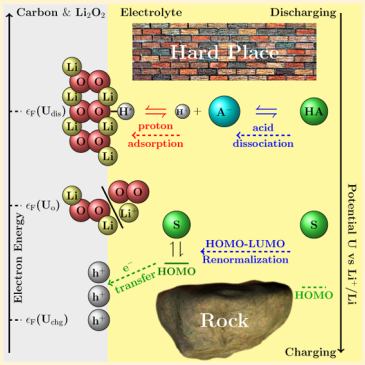

SECTION: Energy Conversion and Storage; Energy and Charge Transport

There has been a tremendous interest in nonaqueous Li–air (or Li-O_2) batteries owing to their high specific energy.[1,2] However, two critical challenges remain, (i) the sudden death during deep discharge due to loss in electronic conductivity of the discharge product,[3−5] which ultimately limits the capacity,[6] and (ii) the decomposition of the electrolyte and carbon cathode, which imposes severe limitations on the rechargeability.[7,8] The development of a rechargeable Li-O_2 battery hinges on the identification of electrolytes that are stable in the electrochemical environment of the Li-O_2 battery.[9−11]

McCloskey et al.[8,12] have demonstrated the importance of quantifying the Li-O_2 electrochemistry by employing differential electrochemical mass spectrometry (DEMS). This has enabled quantification of the parasitic reactivity between Li_2O_2, the desired Li-O_2 battery discharge product, and the nonaqueous electrolytes. In their studies, they have defined and made use of intuitive and powerful measures of cell performance, number of electrons per O_2 transferred during discharge (e^-/ORR) and charge (e^-/OER).[12] Ideally, both the formation and decomposition of Li_2O_2 should yield $2e^-$ per O_2 molecule.

However, during charge, this number deviates significantly from $2e^-$ per O_2 molecule, and this formed the focus of our earlier investigation.[13] In our earlier work, on the basis of a systematic treatment of the electrochemical environment of Li_2O_2, we proposed that, to a first approximation, the HOMO level of the solvent molecule in vacuum could serve as a descriptor for oxidative stability. Using this descriptor, we screened a large number of solvents for their desirable stability characteristics during oxidation.

During discharge in nonaqueous Li-O_2 batteries, several nonaqueous solvents, such as dimethoxyethane (DME), dimethyl sulfoxide (DMSO), *N*-methylpyrrolidone (NMP), tetrahydrofuran (THF), acetonitrile (MeCN), and so forth, yield a $2e^-$ per O_2 value within nominal experimental error (Table S1, Supporting Information). However, this only guarantees that the overall reduction process yields $2e^-$ per O_2 and does not guarantee that all of the electrons lead to the desirable discharge product, Li_2O_2. On the basis of a newly developed iodometric titration protocol, McCloskey et al.[12] showed that even in the "most stable" solvent, DME, the maximum yield of Li_2O_2 is only 91% of the expected, owing to parasitic processes that result in formation of hydrogenated byproducts such as $LiHCO_2$.[12]

In this work, building on our earlier analysis, we formulate a more complete picture of solvent stability during both discharge and charge. We demonstrate that the solvent's propensity to resist H-abstraction induced due to adsorption at the Li_2O_2/carbon interface during discharge is determined by its acid dissociation constant, pK_a, in its own environment. We construct a stability plot of the solvent's HOMO level and its pK_a in DMSO, wherein the stable solvents must possess low HOMO levels and high pK_a. However, it is observed that most solvents show a correlated behavior between its HOMO level

Received: June 6, 2014
Accepted: June 23, 2014
Published: June 23, 2014

   dx.doi.org/10.1021/jz501154v | *J. Phys. Chem. Lett.* 2014, 5, 2419−2424

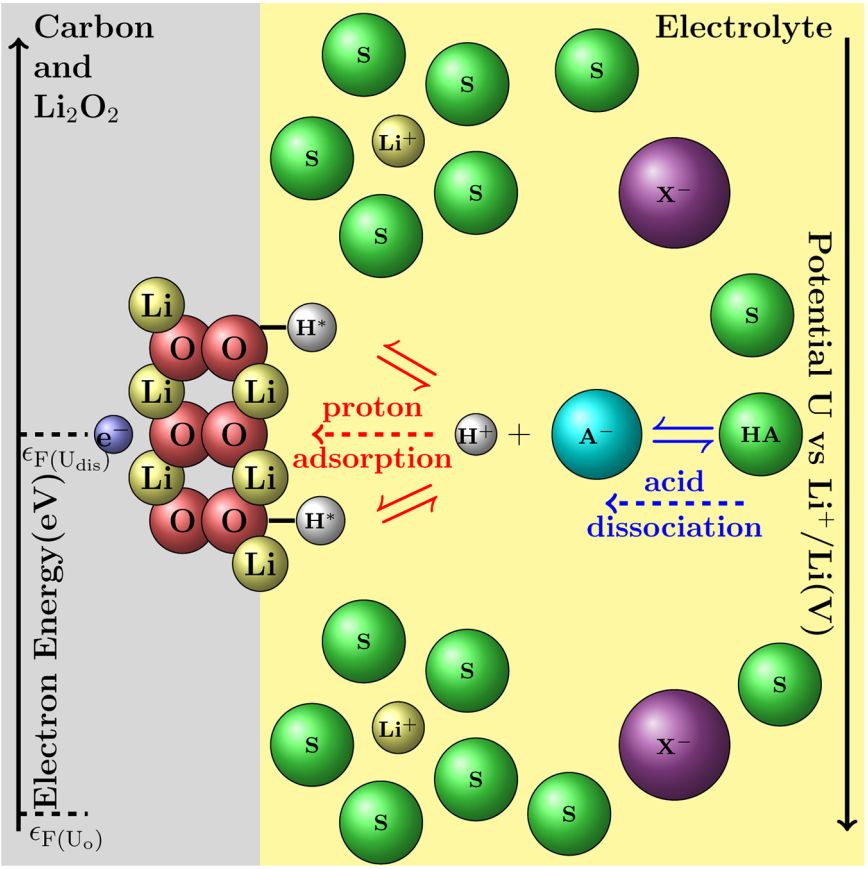

Figure 1. Schematic showing H-abstraction induced due to H adsorption by the Li_2O_2/carbon cathode interface. The molecules denoted in green are the nonaqueous solvent molecules, S. The solvent molecule is also denoted as a weak acid, HA, which is in equilibrium with its conjugate base, A^-, and proton, H^+. The protons are further shown to be in equilibrium with the Li_2O_2/carbon cathode interface where they can be adsorbed at multiple possible sites. Also shown in purple are the solvated Li salt anions, X^-, which are generally much larger in size. On the right side is the potential scale with respect to the Li^+/Li redox couple, and on the left side is the scale denoting the energy of the electron at $\epsilon_{F(U_{dis})}$ while taking part in the electrochemical adsorption reaction at a given discharge potential U_{dis}.

and pK_a. Solvents with lower HOMO levels also possess lower pK_a values, thus implying that the desired stable solvents would have to be outliers to this correlation. This analysis forms the quantitative version of the fundamental trade-off between oxidative stability and H-abstraction suggested earlier.[8]

The formation of Li–H byproducts can take place at the Li_2O_2/carbon interface, where interactions between Li, H, and the carbon cathode are possible. The source of H atoms that take part in these parasitic reactions in the nonaqueous Li-O_2 battery is the electrolyte that consists of the lithium salt and the nonaqueous solvent. Nonaqueous solvents are known to behave akin to nonpolar or weakly polar acids of the form HA, which undergo an acid dissociation process, resulting in protons and the conjugate base A^-, as given in eq 1.

$$HA \leftrightharpoons H^+ + A^- \tag{1}$$

H-abstraction from nonaqueous solvents can be induced due to nucleophilic attack by the O_2^- anion and also due to adsorption at the Li_2O_2/carbon cathode surface. H-abstraction due to nucleophilic attack has been explored in great detail previously by Bryantsev et al.,[14−17] where they showed that such a process of solvent degradation was directly related to the solvent's pK_a. It is worth highlighting that the generation of an O_2^- nucleophile could lead to other parasitic processes, for example, formation of sulfones from DMSO. In this work, we focus on solvent stability against adsorption-induced H-abstraction. The adsorption of protons can be described by eq 2, where $*_{Li_2O_2}$ is the adsorption site on the Li_2O_2 surface, $H^+(HA)$ is the HA solvated proton, and $H^{*Li_2O_2}$ is the H atom adsorbed on the Li_2O_2 surface. The analysis presented here will be analogous in the case that the proton gets adsorbed on any other surface site. The H-abstraction mechanism can be described as competition between the dissociation and the adsorption processes, as illustrated schematically in Figure 1.

$$*_{Li_2O_2} + e^- + H^+(HA) \leftrightharpoons H^{*Li_2O_2} \tag{2}$$

To examine the propensity of H-abstraction via adsorption, we consider the Gibbs free energy of the electrochemical reaction (eq 2), ΔG, as shown in eq 3, where $\Delta G_{H^*(Li_2O_2)}$ is the free energy of the hydrogen adsorbed at the Li_2O_2 interface, $\Delta G_{H^+(HA)}$ is the free energy of the proton solvated by HA, and $\Delta G_{e^-(U_{dis})}$ is the free energy of the electron at the cathode at a given discharge potential U_{dis} (versus Li^+/Li in HA).

$$\Delta G_{(2)} = \Delta G_{H^*Li_2O_2} - \Delta G_{H^+(HA)} - \Delta G_{e^-(U_{dis})} \tag{3}$$

Computationally, the free energy of the protons and electrons in their standard states can be related to the free energy of hydrogen gas at equilibrium conditions in a standard hydrogen electrode (SHE).[18] As given in eq 4, $\Delta G^\circ_{H_2}$ is the free energy of H_2 gas at p = 1 atm and T = 298.15 K, $\Delta G^\circ_{H^+(aq)}$ is the

dx.doi.org/10.1021/jz501154v | J. Phys. Chem. Lett. 2014, 5, 2419−2424

free energy of protons at concentration $[H^+]$ = 1 M in water, and $\Delta G^{\circ}_{e^-}$ is the free energy of electrons at the electrode potential U^{SHE} = 0.

$$\frac{1}{2}\Delta G^{\circ}_{H_2} = \Delta G^{\circ}_{H^+(aq)} + \Delta G^{\circ}_{e^-} \tag{4}$$

In order to use these standard free energies of protons and electrons in eq 3, thermodynamic corrections due to activity of protons in the electrolyte, $kT\ln(a_{H^+(HA)})$, changes in the solvation environment of protons from $[H^+]$ = 1 M in water to $[H^+]$ = 1 M in HA, $\Delta G^{aq\rightarrow HA}_{H^+}$, and the shift in the free energy of electrons due to the electrode potential, $\Delta G_{e^-(U)}$, need to be included. Upon including these corrections, the free energy of protons and electrons in eq 3 can be represented as given in eq 5.

$$\begin{aligned}\Delta G_{H^+(HA)} + \Delta G_{e^-(U_{dis})} &= \Delta G^{\circ}_{H^+(aq)} + \Delta G^{aq\rightarrow HA}_{H^+} + kT\ln(a_{H^+(HA)}) + \Delta G^{\circ}_{e^-} \\ &\quad + \Delta G_{e^-(U)}\end{aligned} \tag{5}$$

The free energy of the electron shifts by an amount $\Delta G_{e^-(U)} = -eU^{SHE}_{dis}$, where U^{SHE}_{dis} is the electrode potential with respect to SHE during discharge. U^{SHE}_{dis} can be expressed as $U^{SHE}_{dis} = U_{dis} + U^{SHE}_{Li^+(HA)/Li}$, where $U^{SHE}_{Li^+(HA)/Li}$ is the equilibrium potential of the Li^+/Li electrode in different solvents with respect to SHE, where U_{dis} is now measured with respect to Li^+/Li. It is well known that the half-wave potentials of the Li^+/Li couples vary across different nonaqueous solvents.[19−23] The location of the half-wave potential is determined by the solvent's ability to solvate Li^+ cations, and this has been found to be well correlated with the Gutmann donor number (DN) of the solvent[20,21] (Figure S1 and Table S2, Supporting Information). In the DN range of 10−30, we observe a linear dependence of the half-wave potential on the DN, and beyond a DN of 30, we observe a saturation in Li^+ solvation. Thus, the value of the equilibrium potential Li^+/Li electrode in a nonaqueous environment with respect to SHE can be expressed as a function of its DN (Supporting Information sections III and VII). Therefore, the shift in the free energy of the electron can be expressed as $\Delta G_{e^-(U)} = -e(U_{dis} + U^{SHE}_{Li^+(HA)/Li}) = -e[U_{dis} + f_{hw}(DN)]$.

Similarly, there will be an effect of the change in the solvation environment of the proton from aqueous to HA. This will also be directly proportional to the DN of the solvent. This is substantiated by the change in free energy of the proton in MeCN (DN = 14.1 kcal/mol, $\Delta G^{aq\rightarrow MeCN}_{H^+}$ = 0.247 eV) and DMSO (DN = 29.8 kcal/mol, $\Delta G^{aq\rightarrow DMSO}_{H^+}$ = −0.278 eV)[24] (Supporting Information section V). We assume the change in energy due to change in solvation environment of protons for any solvent to be a linear function of its DN as $\Delta G^{aq\rightarrow HA}_{H^+} = f_{sol}(DN)$ (Supporting Information sections V and VII). Finally, using the corrections from eq 5, the Gibbs free energy change of H-adsorption is given by eq 6.

$$\begin{aligned}\Delta G_{(2)} = \Delta G_{H^*{}^{Li_2O_2}} - \frac{1}{2}\Delta G^{\circ}_{H_2} - f_{sol}(DN) \\ - kT\ln(a_{H^+(HA)}) + e[U_{dis} + f_{hw}(DN)]\end{aligned} \tag{6}$$

To account for the proton's activity in the nonaqueous solvent, we look at its acid dissociation constant, pK_a, which is defined as

$$pK_a = -\log_{10}(K_a) = -\log_{10}\left(\frac{[H^+][A^-]}{[HA]}\right) \tag{7}$$

Further, assuming $[H^+] = [A^-]$, the expression for pK_a from eq 7 can be substituted into eq 6 to give eq 8 as

$$\begin{aligned}\Delta G_{(2)} = \Delta G_{H^*{}^{Li_2O_2}} - \frac{1}{2}\Delta G^{\circ}_{H_2} - f_{sol}(DN) \\ - \frac{kT}{2}[\ln([HA]) - \ln(10)^*pK_a] + e[U_{dis} + f_{hw}(DN)]\end{aligned} \tag{8}$$

For a given acid HA, pK_a is usually defined using a standard activity (for, e.g., 1 M) of that acid in another medium such as DMSO, MeCN, water, and so forth. However, as can be observed in eq 8, the pK_a values required to ascertain the protons' activity using eq 7 need to be defined with medium being the solvent (acid) itself. Due to technical challenges in measuring proton concentration in nonaqueous solvents, there is a dearth of such exact data in the literature.[25] In order to overcome this problem, we make arguments based on solvation of protons in polar and nonpolar solvents. Physically, the equilibrium between H^+, A^-, and HA can be understood as a competition between the degree of solvation of H^+ and A^- and the chemical bond energy between H and A in the solvent molecule.

Arguably, a higher solvation, and thus stabilization, of H^+ and A^- in a given environment would result in higher auto-ionization of the acid, resulting in lower pK_a values. While the proton is very well solvated in highly polar solvents such as water due to hydrogen bonding, its solvation in nonpolar solvents is not as effective. To explore this solvation effect in detail, we surveyed hundreds of solvents for their pK_a values defined in various media such as dichloroethane (DCE), DME, THF, DMSO, MeCN, and water. As can be seen in Figures S4a−S4e (Supporting Information), there exists a linear correlation between the pK_a values across various classes of solvents in any two given media. Further, the slope of the corresponding lines is often close to 1, with the largest intercept on the order of $\Delta pK_a \approx 10$. This closely correlated behavior can be explained on the basis of a similar degree of relative solvation of protons by all weakly polar or nonpolar solvents and can be utilized in the present analysis. Keeping in mind that a variation on the order of $\Delta pK_a \approx 10$ would result in an error of $(1/2)kT^*\ln(10)^*\Delta pK_a \approx 0.25$ eV in our estimations of the Gibbs free energy from eq 8, we argue that the required pK_a values can all be chosen with respect to one of the media without losing any qualitative features of the model. In this study, we use DMSO as the common medium for the pK_a values.

Using averaged values of ln[HA], $\Delta G^{aq\rightarrow HA}_{H^+}$, and $U^{SHE}_{Li^+(HA)/Li}$, which are calculated using data from commonly used nonaqueous solvents such as DMSO, MeCN, DME, NMP, dimethylacetamide (DMA), and dimethylformamide (DMF), and using a value for $\Delta G_{H^*(Li_2O_2)} - (1/2)\Delta G^{\circ}_{H_2} = -1.5$ eV, we plot a contour map of the Gibbs free energy of the adsorption-induced H-abstraction process, $\Delta G_{(2)}$, as a function of solvent's calculated pK_a in DMSO and their DN values in Figure 2. The values are shown relative to that of MeCN, which has the lowest pK_a among the solvents considered. The Gibbs free energy changes weakly with the solvent's DN. This is due to a cancellation between the solvation of Li^+ and H^+. It can therefore be deduced that the main influencing factor deciding

dx.doi.org/10.1021/jz501154v | J. Phys. Chem. Lett. 2014, 5, 2419−2424

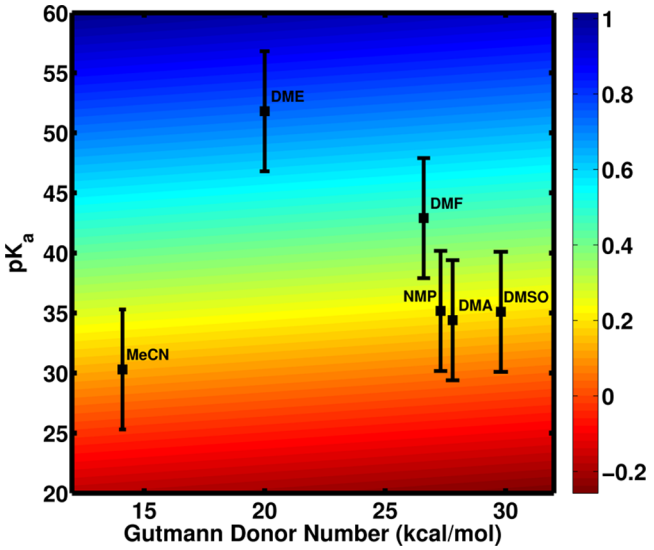

Figure 2. Contour map showing the variation of the change in Gibbs free energy during the adsorption-induced H-abstraction process, $\Delta G_{(2)}$, as a function of the solvent's acid dissociation constant, pK_a, and the DN. The Gibbs free energy values are shown relative to that of MeCN, which has the lowest pK_a value. Locations of solvents, DMSO (pK_a = 35.1, DN = 29.8 kcal/mol), MeCN (pK_a = 30.3, DN = 14.1 kcal/mol), DME (pK_a = 51.8, DN = 20.0 kcal/mol), NMP (pK_a = 35.2, DN = 27.3 kcal/mol), DMF (pK_a = 42.9, DN = 26.6 kcal/mol), and DMA (pK_a = 34.4, DN = 27.8 kcal/mol), are shown on the map using their calculated pK_a values in DMSO[15−17] and their DNs.[28,29] The map has been plotted using eq 8 with the values for ln[HA] = 2.52, $\Delta G_{H^+}^{aq\rightarrow HA}$ = −0.09 eV, and $U_{Li^+(HA)/Li}^{SHE}$ = 2.08 V, which are the averages of the values for all of the shown solvents, computed using linear interpolation as a function of DN whenever unavailable (section VII and Table S4, Supporting Information). The value for $\Delta G_{H^*(Li_2O_2)} - (1/2)(\Delta G^{\circ}_{H_2})$ was set to −1.5 eV. The contour map clearly demonstrates why pK_a is the most important deciding factor for stability against H-abstraction. The Gibbs free energy changes weakly with the solvent's DN, which implies a cancellation of the effect of the solvation of Li^+ and H^+.

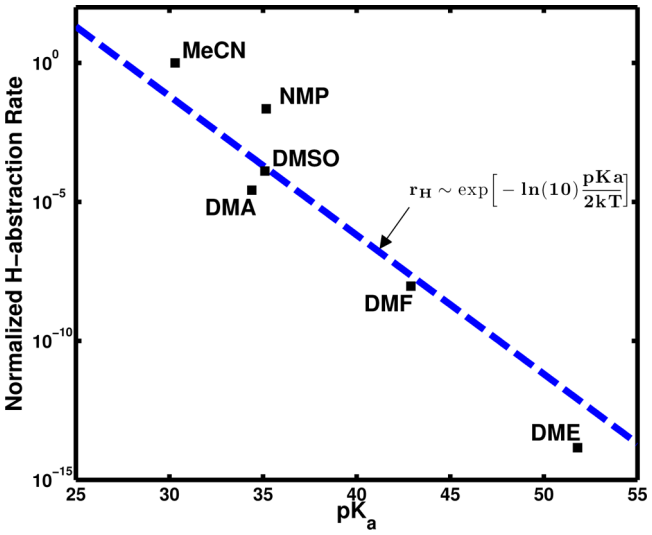

Figure 3. Figure showing the rate of H-abstraction, $r_H \approx \exp[-\ln(10)*(pK_a/2kT)]$, as a function of the solvent's acid dissociation constant, pK_a, at a fixed discharge potential, U_{dis} = 2.67 V (dashed blue line). The value has been normalized with respect to the rate value for MeCN, which has the lowest pK_a value among the considered solvents. Locations of the calculated rates of H-abstraction for solvents, DMSO (U_{dis} = 2.7 V, pK_a = 35.1), MeCN (U_{dis} = 2.55 V, pK_a = 30.3), DME (U_{dis} = 2.75 V, pK_a = 51.8), NMP (U_{dis} = 2.55 V, pK_a = 35.17), DMF (U_{dis} = 2.7 V, pK_a = 42.9), and DMA (U_{dis} = 2.75 V, pK_a = 34.4), are shown on the map using their calculated pK_a values in DMSO[15−17] and their approximate discharge potentials measured experimentally.[12,30−32] The line representing r_H has been calculated using eq 8 with the values for ln[HA] = 2.52, $\Delta G_{H^+}^{aq\rightarrow HA}$ = −0.09 eV, and $U_{Li^+(HA)/Li}^{SHE}$ = 2.08 V, which are the averages of the values for all of the shown solvents, computed using linear interpolation as a function of DN whenever unavailable (section VII and Table S4, Supporting Information). The value for $\Delta G_{H^*(Li_2O_2)} - (1/2)(\Delta G^{\circ}_{H_2})$ was set to −1.5 eV. As can be observed, despite using averaged values for $\Delta G_{H^+}^{aq\rightarrow HA}$, $U_{Li^+(HA)/Li}^{SHE}$, ln[HA], and pK_a for all solvents in DMSO, the model predicts well the variation in the rate of H-abstraction due to pK_a using the thermodynamic analysis developed in this study.

the propensity of the H-abstraction process is the solvent's pK_a. It must be noted that with an increase in the discharging overpotential, the rate of the H-abstraction process will be accelerated. However, it has been observed that the discharge potential in various solvents is similar.[12,26,27]

In order to analyze the effect of the assumptions made in the theoretical model, we calculate the rate for H-abstraction, $r_H \approx \exp[-\ln(10)*(pK_a/2kT)]$, as a function of the solvent's acid dissociation constant, pK_a, at a fixed discharge potential, U_{dis} = 2.67 V. The rate has been normalized with respect to the rate value for MeCN, which has the lowest pK_a among the solvents considered. Figure 3 shows the logarithmic variation of r_H with respect to solvent's pK_a, where the medium is the solvent itself, calculated using averaged values of ln[HA], $\Delta G_{H^+}^{aq\rightarrow HA}$, and $U_{Li^+(HA)/Li}^{SHE}$. In the same plot, the calculated rates for solvents such as DMSO, MeCN, DME, NMP, DMA, and DMF, using their exact values for ln[HA], $\Delta G_{H^+}^{aq\rightarrow HA}$, $U_{Li^+(HA)/Li}^{SHE}$, and U_{dis}, and their calculated pK_a's in DMSO are shown. The model reproduces the trends for H-abstraction well. Also, it can be observed that the assumption of choosing pK_a values defined in a single medium does not have a major effect on the relative trends across solvents.

Finally, in Figure 4, we plot the overall solvent stability visualized as functions of the HOMO level, which is the descriptor of solvent stability against oxidation during charge, and pK_a in DMSO, which is a good approximation for solvent stability against H-abstraction during discharge. We divide the stability plot into four quadrants, where the HOMO level benchmark is set using the calculated value for the HOMO level of DME = −11.44 eV, and the pK_a benchmark is set using the calculated value in DMSO for MeCN ≈ 30. The desired solvents need to have a HOMO level lower than −11.44 eV and a pK_a more than 30. This plot shows that DME strikes the right balance between oxidative stability and H-abstraction and appears to be the most stable among the common organic solvents. As can be seen, there are very few other compounds in the top left quadrant such as methane, methyl acetate, methylpivalate, and propionitrile that satisfy these minimum requirements. For most solvents, there exists a correlation between the two stability descriptors. This implies that solvents having a deep HOMO level also have a low pK_a. However, a low value of the HOMO level and a high value of pK_a are desired for overall solvent stability. This implies that solvents with the desired stability characteristics have to be outliers to this correlation. The plot forms the quantitative version of the fundamental trade-off between oxidative stability and H-

dx.doi.org/10.1021/jz501154v | J. Phys. Chem. Lett. 2014, 5, 2419−2424

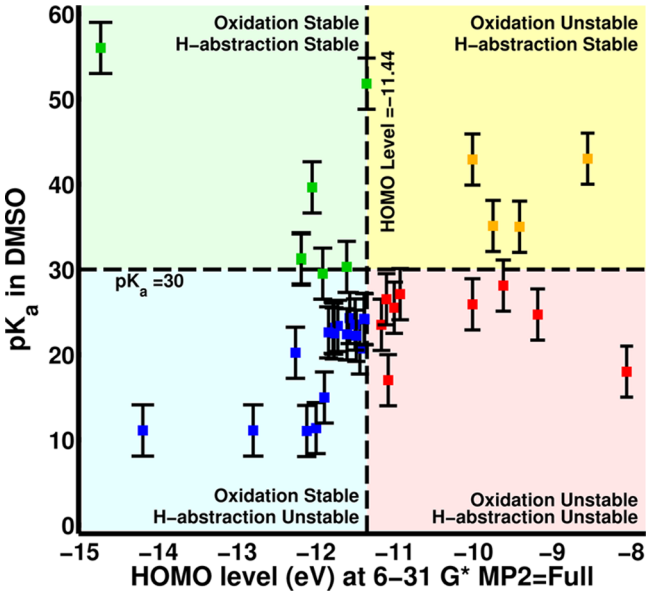

Figure 4. Regions of solvent stability visualized as functions of the HOMO level, which is the descriptor of solvent stability against oxidation during charge, and pK_a in DMSO, which is a good approximation to the descriptor for stability against H-abstraction during discharge. The figure is divided into four quadrants, where the HOMO level benchmark is set using the calculated value for the HOMO level of DME = −11.44 eV, and the pK_a benchmark is set using the calculated value in DMSO for MeCN ≈ 30. The top left quadrant represents the zone of solvents that can be expected to be relatively stable against both oxidation and H-abstraction. The top right quadrant represents the zone of solvents that will probably be stable against H-abstraction but unstable against oxidation during charging. Likewise, the bottom left quadrant represents the zone of solvents that are probably stable against oxidation but unstable against H-abstraction. Finally, the bottom right quadrant represents the zone of solvents that can be expected to be unstable against both oxidation and H-abstraction. As can be observed, there exists a correlation between the two stability descriptors. The figure is a quantitative version of the stability trade-off hypothesis,[8] clearly indicating why there is a dearth of solvents that are stable against both oxidation and H-abstraction. The complete list of solvents in this figure and their corresponding pK_a and HOMO level values along with the references are given in Table S3 (Supporting Information).

abstraction.[8] The complete list of solvents in this plot and their corresponding pK_a and HOMO level values along with the references are given in Table S3 (Supporting Information).

This work outlines the stringent stability requirements imposed on the solvent for nonaqueous Li-O_2 batteries. Additionally, solvents for practical Li-O_2 battery applications will need to satisfy several other criteria like Li salt and O_2 solubility, high ionic conductivity, and stability against the Li metal anode. This highlights the need for a beyond brute-force rational search of solvents, and we believe computation will play a crucial role in ultimately identifying the blend of solvents required for a practical nonaqueous Li-O_2 battery. In an effort to accelerate the discovery of this stable electrolyte, we have developed an easily queryable "electrolyte genome" (see the Supporting Information), and all of the data presented here are made available. We believe that such a genome will prove extremely useful and enable toward a rational design of electrolytes.

■ ASSOCIATED CONTENT

Supporting Information

(I) Indicators of solvent performance during charge and discharge, their HOMO levels, and Gutmann donor numbers (DNs). (II) Half-wave potential of the Li^+/Li redox couple in various solvents. (III) Estimation of the location of the Li^+/Li redox couple in different nonaqueous solvents with respect to the standard hydrogen electrode (SHE), $U^{SHE}_{Li^+_{(HA)/Li}}$. (IV) Correlations between pK_a values of solvents in various media. (V) Calculation of the change in energy of the proton upon a change in the solvation environment from aqueous to a given nonaqueous one, $\Delta G^{aq\rightarrow HA}_{H^+}$. (VI) Data for HOMO values and pK_a values in DMSO for solvents in the stability plot (Figure 4). (VII) Interpolation of values for the location of the Li^+/Li couple in HA with respect to SHE, $U^{SHE}_{Li^+_{(HA)/Li}}$, and the change in energy due to change in the solvation environment from aqueous to HA, $\Delta G^{aq\rightarrow HA}_{H^+}$, using DNs. (VIII) Electrolyte genome. This material is available free of charge via the Internet at http://pubs.acs.org.

■ AUTHOR INFORMATION

Corresponding Author

*E-mail: venkvis@cmu.edu.

Notes

The authors declare no competing financial interest.

■ ACKNOWLEDGMENTS

The authors acknowledge helpful discussions with Alan Luntz and Bryan McCloskey. A.K. thankfully acknowledges the funding for his doctoral studies by the Deutsche Forschungsgemeinschaft (DFG).

■ REFERENCES

(1) Girishkumar, G.; McCloskey, B.; Luntz, A. C.; Swanson, S.; Wilcke, W. Lithium-Air Battery: Promise and Challenges. *J. Phys. Chem. Lett.* **2010**, *1*, 2193−2203.

(2) Bruce, P. G.; Freunberger, S. A.; Hardwick, L. J.; Tarascon, J.-M. Li-O_2 and Li−S Batteries with High Energy Storage. *Nat. Mater.* **2012**, *11*, 19−29.

(3) Viswanathan, V.; Thygesen, K. S.; Hummelshøj, J. S.; Nørskov, J. K.; Girishkumar, G.; McCloskey, B. D.; Luntz, A. C. Electrical Conductivity in Li_2O_2 and Its Role in Determining Capacity Limitations in Non-Aqueous Li-O_2 Batteries. *J. Chem. Phys.* **2011**, *135*, 214704.

(4) Viswanathan, V.; Nørskov, J. K.; Speidel, A.; Scheffler, R.; Gowda, S.; Luntz, A. C. Li-O_2 Kinetic Overpotentials: Tafel Plots from Experiment and First-Principles Theory. *J. Phys. Chem. Lett.* **2013**, *4*, 556−560.

(5) Varley, J. B.; Viswanathan, V.; Nørskov, J. K.; Luntz, A. C. Lithium and Oxygen Vacancies and Their Role in Li_2O_2 Charge Transport in Li-O_2 Batteries. *Energy Environ. Sci.* **2014**, *7*, 720−727.

(6) Luntz, A. C.; Viswanathan, V.; Voss, J.; Varley, J. B.; Nørskov, J. K.; Scheffler, R.; Speidel, A. Tunneling and Polaron Charge Transport through Li_2O_2 in Li-O_2 Batteries. *J. Phys. Chem. Lett.* **2013**, *4*, 3494−3499.

(7) Peng, Z.; Freunberger, S. A.; Hardwick, L. J.; Chen, Y.; Giordani, V.; Bardé, F.; Novák, P.; Graham, D.; Tarascon, J.-M.; Bruce, P. G. Oxygen Reactions in a Non-Aqueous Li^+ Electrolyte. *Angew. Chem., Int. Ed.* **2011**, *50*, 6351−6355.

(8) McCloskey, B. D.; Bethune, D. S.; Shelby, R. M.; Mori, T.; Scheffler, R.; Speidel, A.; Sherwood, M.; Luntz, A. C. Limitations in Rechargeability of Li-O_2 Batteries and Possible Origins. *J. Phys. Chem. Lett.* **2012**, *3*, 3043−3047.

(9) Lu, Y.-C.; Gallant, B. M.; Kwabi, D. G.; Harding, J. R.; Mitchell, R. R.; Whittingham, M. S.; Shao-Horn, Y. Lithium-Oxygen Batteries: Bridging Mechanistic Understanding and Battery Performance. *Energy Environ. Sci.* **2013**, *6*, 750−768.
(10) Balaish, M.; Kraytsberg, A.; Ein-Eli, Y. A Critical Review on Lithium-Air Battery Electrolytes. *Phys. Chem. Chem. Phys.* **2014**, *16*, 2801−2822.
(11) Ottakam Thotiyl, M. M.; Freunberger, S. A.; Peng, Z.; Bruce, P. G. The Carbon Electrode in Nonaqueous Li-O_2 Cells. *J. Am. Chem. Soc.* **2013**, *135*, 494−500.
(12) McCloskey, B. D.; Valery, A.; Luntz, A. C.; Gowda, S. R.; Wallraff, G. M.; Garcia, J. M.; Mori, T.; Krupp, L. E. Combining Accurate O_2 and Li_2O_2 Assays to Separate Discharge and Charge Stability Limitations in Nonaqueous Li-O_2 Batteries. *J. Phys. Chem. Lett.* **2013**, *4*, 2989−2993.
(13) Khetan, A.; Pitsch, H.; Viswanathan, V. Identifying Descriptors for Solvent Stability in Nonaqueous Li-O_2 Batteries. *J. Phys. Chem. Lett.* **2014**, *5*, 1318−1323.
(14) Bryantsev, V. S.; Blanco, M. Computational Study of the Mechanisms of Superoxide-Induced Decomposition of Organic Carbonate-Based Electrolytes. *J. Phys. Chem. Lett.* **2011**, *2*, 379−383.
(15) Bryantsev, V. S.; Faglioni, F. Predicting Autoxidation Stability of Ether- and Amide-Based Electrolyte Solvents for Li-Air Batteries. *J. Phys. Chem. A* **2012**, *116*, 7128−7138.
(16) Bryantsev, V. S. Predicting the Stability of Aprotic Solvents in Li-Air Batteries: pK_a Calculations of Aliphatic C−H Acids in Dimethyl Sulfoxide. *Chem. Phys. Lett.* **2013**, *558*, 42−47.
(17) Bryantsev, V. S.; Uddin, J.; Giordani, V.; Walker, W.; Addison, D.; Chase, G. V. The Identification of Stable Solvents for Nonaqueous Rechargeable Li-Air Batteries. *J. Electrochem. Soc.* **2013**, *160*, A160−A171.
(18) Nørskov, J. K.; Rossmeisl, J.; Logadottir, A.; Lindqvist, L.; Kitchin, J. R.; Bligaard, T.; Jonsson, H. Origin of the Overpotential for Oxygen Reduction at a Fuel-Cell Cathode. *J. Phys. Chem. B* **2004**, *108*, 17886−17892.
(19) Connelly, N. G.; Geiger, W. E. Chemical Redox Agents for Organometallic Chemistry. *Chem. Rev.* **1996**, *96*, 877−910.
(20) Gritzner, G. Polarographic Half-Wave Potentials of Cations in Nonaqueous Solvents. *Pure Appl. Chem.* **1990**, *62*, 1839−1858.
(21) Gritzner, G.; Lewandowski, A. Temperature Coefficients of Half-Wave Potentials and Entropies of Transfer of Cations in Aprotic Solvents. *J. Chem. Soc., Faraday Trans.* **1991**, *87*, 2599−2602.
(22) Laoire, C. O.; Mukerjee, S.; Abraham, K. M.; Plichta, E. J.; Hendrickson, M. A. Elucidating the Mechanism of Oxygen Reduction for Lithium-Air Battery Applications. *J. Phys. Chem. C* **2009**, *113*, 20127−20134.
(23) Laoire, C. O.; Mukerjee, S.; Abraham, K. M.; Plichta, E. J.; Hendrickson, M. A. Influence of Nonaqueous Solvents on the Electrochemistry of Oxygen in the Rechargeable Lithium-Air Battery. *J. Phys. Chem. C* **2010**, *114*, 9178−9186.
(24) Marenich, A. V.; Kelly, C. P.; Thompson, J. D.; Hawkins, G. D.; Chambers, C. C.; Giesen, D. J.; Winget, P.; Cramer, C. J.; Truhlar, D. G. *Minnesota Solvation Database* , version 2012; University of Minnesota: Minneapolis, MN, 2012.
(25) Cookson, R. F. Determination of Acidity Constants. *Chem. Rev.* **1974**, *74*, 5−28.
(26) Jung, H.-G.; Hassoun, J.; Park, J.-B.; Sun, Y.-K.; Scrosati, B. An Improved High-Performance Lithium-Air Battery. *Nat. Chem.* **2012**, *4*, 579−585.
(27) Peng, Z.; Freunberger, S. A.; Chen, Y.; Bruce, P. G. A Reversible and Higher-Rate Li-O_2 Battery. *Science* **2012**, *337*, 563−566.
(28) Gutmann, V. Solvent Effects on the Reactivities of Organometallic Compounds. *Coord. Chem. Rev.* **1976**, *18*, 225−255.
(29) Mayer, U. A Semiempirical Model for the Description of Solvent Effects on Chemical Reactions. *Pure Appl. Chem.* **1979**, *51*, 1697−1712.
(30) Chen, Y.; Freunberger, S. A.; Peng, Z.; Bard, F.; Bruce, P. G. Li-O_2 Battery with a Dimethylformamide Electrolyte. *J. Am. Chem. Soc.* **2012**, *134*, 7952−7957.
(31) Bryantsev, V. S.; Giordani, V.; Walker, W.; Uddin, J.; Lee, I.; van Duin, A. C. T.; Chase, G. V.; Addison, D. Investigation of Fluorinated Amides for Solid-Electrolyte Interphase Stabilization in Li-O_2 Batteries Using Amide-Based Electrolytes. *J. Phys. Chem. C* **2013**, *117*, 11977−11988.
(32) Walker, W.; Giordani, V.; Uddin, J.; Bryantsev, V. S.; Chase, G. V.; Addison, D. A Rechargeable Li-O_2 Battery Using a Lithium Nitrate/*N*,*N*-Dimethylacetamide Electrolyte. *J. Am. Chem. Soc.* **2013**, *135*, 2076−2079.